76th International Astronautical Congress (IAC), Sydney, Australia, 29 September to 03 October 2025.

IAC-25,E2,3-GTS.4,9,x99868

BEYOND ABLATION: INTEGRATING ACTIVE COOLING INTO HYBRID HEATSHIELDS FOR NEXT-GEN SPACECRAFT PROTECTION

Patrik Rychtarčík, Lukáš Hudáček, Emanuel Ungero, Jonáš Sarvaš, Patrik Zádrapa, Timotej Kojš, Andrii Hrytchuk, Barbora Stupavská, Daniel Kóňa, Martin Konečný, Pavlo Usatiuk, Peter Gornyitzki, Sebastián Hudák[a]

[a] *Faculty of Aeronautics, Technical University of Košice, Slovakia, harts.rexus@gmail.com*

Abstract

Reusable thermal protection remains a fundamental challenge in operating sustainable spacecraft during the harsh conditions of atmospheric re-entry, where both reliability and lightweight structure play a critical role. To this day, no ideal solution has been found in the eld of reusable heatshields. Currently used reusable capacitive tiles have proven to be unreliable and hard to maintain due to their fragile nature, while most ablative systems are not sustainable for prolonged use. This study focuses on the complete design, numerical modelling, and preliminary validation of an experiment module protected by a Hybrid Atmospheric Re-entry Thermal Shield (HARTS). This technology integrates known passive thermal protection systems with an actively cooled layer into a hybrid solution, addressing limitations of currently used heatshields. HARTS explores the concept of using leftover helium from fuel tank pressurization as a coolant. This approach aims to decrease the need for insulation and increase the service life of carbon-resin ablative heatshields without adding extra mass. HARTS is a project led by university students from the Technical University of Kosice, under the administration of the Faculty of Aeronautics and supported by the Slovak Space Office and the Ministry of Education of the Slovak Republic. Team HARTS is participating in Cycle 16 of the international REXUS/BEXUS Student experiment program with the experiment scheduled to fly aboard REXUS 35 in March 2026 from the Esrange Space Center (SSC) in Kiruna, Sweden. The results will provide insights into the feasibility of a hybrid heatshield built on a self-supporting ablative carbon-resin composite structure with integrated coolant distribution piping array. The main goal is to prepare the HARTS experiment module and the hybrid heatshield technology for its launch on a sounding rocket into high altitude and subsequent testing during supersonic atmospheric re-entry. The findings from this experiment will contribute to the advancement of reusable thermal protection systems, providing valuable insight into the development of next-generation spacecraft re-entry technologies.

Keywords: Hybrid Heatshield, Reusable, Carbon-Resin Composite, Active Cooling

Acronyms/Abbreviations

HARTS – Hybrid Atmoshperic Reentry Thermal Shield

REXUS – Rocket Experiments for University Students

FFU- Free falling Unit

RMU – Rocket Mounted Unit

RXSM – REXUS Service Module

CoP – Centre of Pressure

CoG – Centre of Gravity

1. Introduction

The HARTS experiment aims to develop a hybrid re-entry heatshield that combines passive ablation with active cooling to mitigate the shortcomings of each approach. The concept builds on the earlier Active Heatshield Cooling Solutions project, which won the ArianeGroup Prize in the ESA Student Aerospace Challenge 2024, but was limited by high fuel consumption and added mass. Based on feedback from Ariane researchers, the design evolved into HARTS, integrating active cooling into structural ablative composites.

Carbon–phenolic composites offer excellent mechanical strength and potential structural integration, as demonstrated in the ArianeGroup SC-X01 demonstrator and the planned Phoebus capsule. However, their high density, thermal conductivity, and reduced ablation efficiency compared to materials such as PICA or AVCOAT make them less attractive for conventional use.

The hybrid system addresses these drawbacks by circulating helium, already available onboard as a propellant tank pressurant, through channels within the carbon–resin structure. This passive-active

combination reduces insulation needs, extends heatshield lifetime, and avoids significant mass penalties, since no dedicated coolant is required. The design ensures survivability even in case of coolant failure, as the ablative layer remains functional. Because many aerothermal effects cannot be reproduced in laboratories, HARTS will undergo validation in real conditions during a supersonic free-fall flight aboard a REXUS sounding rocket. The results will provide essential data on the feasibility of hybrid TPS (thermal protection systems) technologies for future reusable spacecraft [1].

2. Experiment concept

The mission of HARTS is to test the performance of a hybrid re-entry heatshield under real atmospheric conditions. The system will be validated using the REXUS sounding rocket, which will carry the experiment into high altitude and eject a stabilized capsule into free fall. The capsule will reach supersonic speeds, producing significant aerodynamic heating on a blunt leading surface protected by the HARTS technology.

The HARTS experiment consists of two main units:

- **FFU – Free Falling Unit**: Capsule, with dimensions 150x150x180, containing the hybrid heatshield, regulation system, and all necessary subsystems for communication, power, tracking, data storage, and recovery.
- **Shape adapters –** It wraps around the FFU, locking it in place with an anti-rotation ledge to prevent tilting.
- **RMU – Rocket Mounted Unit**: Ejection system housed within the experiment module, responsible for releasing the FFU and relaying its data to the REXUS Service Module (RXSM). It also charges the FFU batteries before ejection.

Entire experiment setup is shown in Fig. 1.

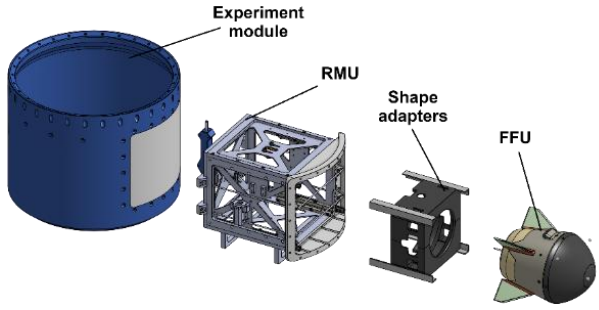

Fig. 1. Experiment setup illustration

Launch

Prior to launch, the FFU is installed within the RMU, which is then mounted inside the experiment module and connected to RXSM. Following pre-launch testing, the ground station instructs the FFU to transition to its internal battery power, placing all subsystems in standby mode until the system receives the lift-off signal. Once lift-off occurs, the system begins collecting sensor data and transmitting it to the ground station via the RXSM.

Ejection

The ejection of the FFU is controlled by the RXSM. At the set altitude, RXSM activates pyro cutters that cut the steel cables holding the RMU hatch, allowing it to detach and spring away. A second pyro cutter then releases a compression spring that pushes the FFU out of the RMU. An onboard RMU camera provides live video through the REXUS TV channel to confirm successful ejection.

Descent

After ejection, the FFU descends on a ballistic path through the atmosphere. At peak heating, helium is released through internal pipes to cool the heatshield. PT1000 sensors embedded in the shield record temperature throughout the fall, while a side-mounted camera captures video of the descent for analysis and outreach. The FFU capsule is stabilized by four fins mounted symmetrically around the body cone and by concentrating mass toward the nose. The fins improve stability by shifting the center of pressure, keeping the capsule aligned during descent.

Parachute Deployment

The FFU uses a built-in parachute to ensure safe landing by reducing its descent speed. Deployment is triggered by the onboard microcontroller once certain conditions are met: the capsule must have risen above 4 km, separation from the RMU must be confirmed, more than 200 seconds must have passed since launch, or the altitude must have dropped below 4 km. When triggered. the cover is pushed away by springs and acts as a pilot chute to pull out the main parachute. Once fully deployed, the parachute slows the capsule to about 9 m/s for a controlled landing.

Touchdown and Recovery

After landing, the recovery team locates the FFU using its last transmitted coordinates, which narrow down the search area. The deployed parachute acts as

a bright visual marker, making the capsule easier to spot from a distance. In case the parachute fails, a passive buzzer provides an audio signal to help locate the capsule on the ground [2].

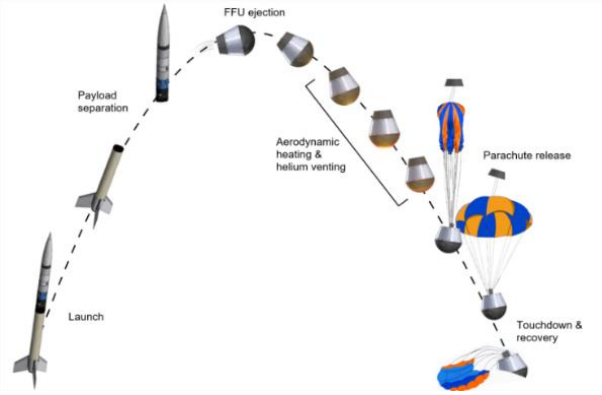

Fig. 2. Experiment timeline

3. RMU

Rocket Mounted Unit is inherited from Team FENRIR, whose design successfully flew in a previous REXUS/BEXUS campaign. For HARTS, the system was further modified to improve accessibility, setup time, and integration with the hybrid heatshield capsule. The ejection system provides the mechanical, electrical, and communication interface between the FFU and the RXSM. It consists of a container, hatch, flange, ejection mechanism, and retention mechanism (See Fig. 3). Most components are made from aluminum (See Fig.4 and Fig.5), while critical parts such as spring mounts, pyro cutters, fixation brackets, bearings, retention cables, rails, and springs use steel or specialized materials. The container is fixed to the bottom bulkhead of the experiment module and houses both the ejection mechanism and the FFU, which is guided during release along rails with bearings to reduce friction.

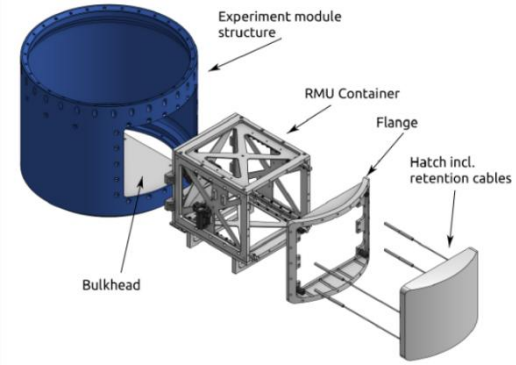

Fig. 3. RMU with experiment module

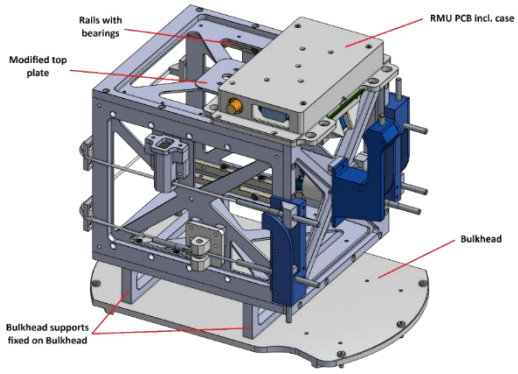

Fig. 4. Back view of RMU

The hatch closes the container while the flange provides the interface between the hatch and the module, with four corner springs supplying ejection force. Openings allow passage of retention cables, and a 2° taper is added to the hatch, flange, and module walls to ease ejection.

The ejection mechanism is designed to release the hatch first and then the FFU. Bearings present at each rail reduce friction during spring-driven ejection. The retention mechanism secures both the hatch and the FFU during ascent. The hatch is restrained by two steel cables with threaded M5 terminals, cable guides, retention brackets, and pyro cutter holders, with ceramic paste applied to reduce friction in the guides. The FFU is held by one additional 2 mm, 7×7 steel cable, fastened between the container and the FFU spring mount.

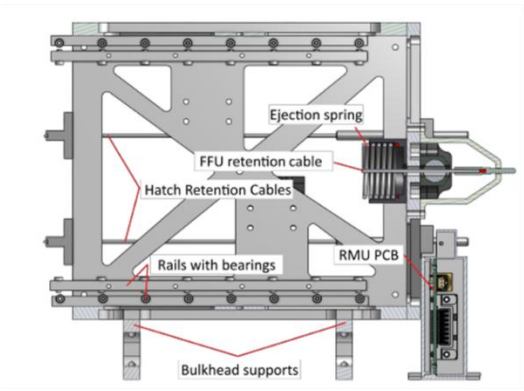

Fig. 5. Cross section of retention mechanism

From the original FENRIR design, HARTS introduced several modifications:

- Retention brackets were rotated (two upwards, one downwards), making them accessible for tightening even with the RMU installed in the experiment module (Fig.6).

- Cable clamps replaced one of the threaded ends, reducing setup time. Although this limits perfectly equal tensioning, positioning the fixed ends opposite each other and balancing torque with a rubber mallet compensates for the difference (Fig 6 and Fig.7).
- A new RMU case was developed to house a redesigned PCB layout with a different communication protocol. The aluminum case improves access to connectors, provides better placement for the onboard camera, and offers radiation shielding.
- A bulkhead cutout was added to allow access to the downward-facing retention mechanism screw terminal.

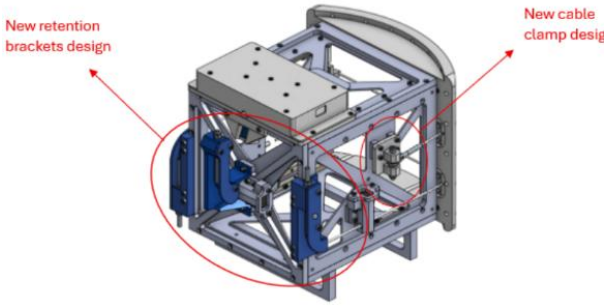

.

Fig. 6. New retention brackets design

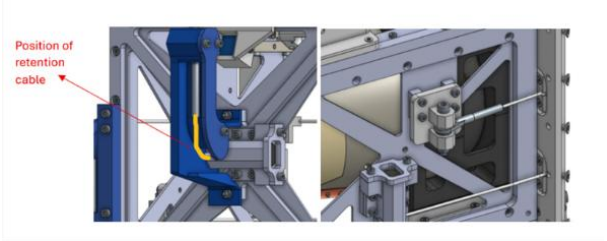

Fig. 7. New FFU retention mechanism

The release mechanism uses three pyro cutters: two cut the hatch retention cables, and one cuts the FFU retention cable. Each cutter is locked into a fixed case to prevent movement. The sequence ensures the hatch is released first, followed shortly by the FFU, and is fully controlled by the REXUS Service module.

Retention system is presented in Fig.8.

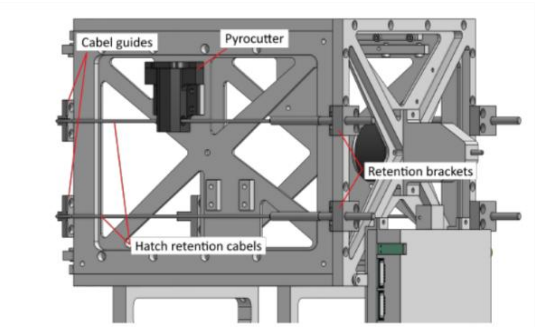

Fig. 8. RMU with retention cable and brackets

Most RMU parts are produced using 5-axis CNC machining from Aluminum 7075, chosen for its high strength and low thermal expansion [3].

4. Shape adapters

The main difference between the inherited FENRIR ejection system and the HARTS design is the addition of a shape adapter (see Fig. 9) to fit the new capsule configuration. The adapter replicates the outer contour of the FFU while forming a cubic outer surface, allowing a secure fit inside the ejection container (See Fig. 10 and Fig. 11).

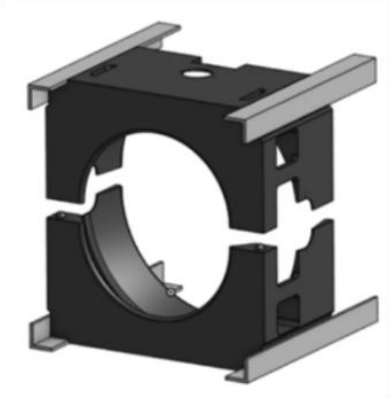

Fig. 9. Shape adapter sub-assembly

The adapter consists of two halves joined by ball pins and sockets. It wraps around the FFU and locks it in place using an anti-rotation ledge that prevents tilting, while a groove on the opposite side houses the PogoPin connector. Four aluminum L-profiles are bonded into the corners to increase stiffness and provide smooth surfaces for the bearings to slide on.

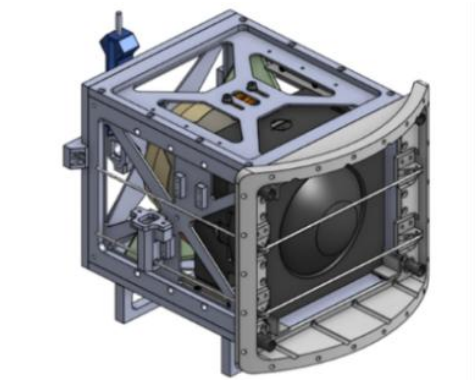

Fig. 10. Isometric view of RMU and FFU with adapters

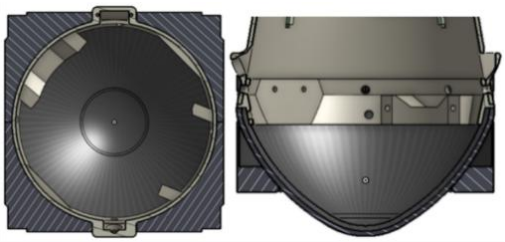

Fig. 11. Cross sections on the groove and ledge

Following a sabot-like concept, the two halves of the adapter separate after ejection, releasing the FFU into free fall. The adapters are not recovered and are discarded after use. TPU 95A was selected as the material due to its toughness and high friction coefficient, ensuring both durability and stability during ejection [4].

5. FFU

Free Falling Unit (FFU) is divided into three main components (shown in Fig.12), each serving a specific role to ensure mission success. Together, they guarantee that the system performs as intended.

- **Recovery System** – Ensures a safe and controlled landing of the module after experiment completion.
- **Module Bay** – Functions as the central hub, housing all key systems and components required for operation.
- **Heatshield** – Serves as the primary test article, designed to evaluate and validate thermal protection performance.

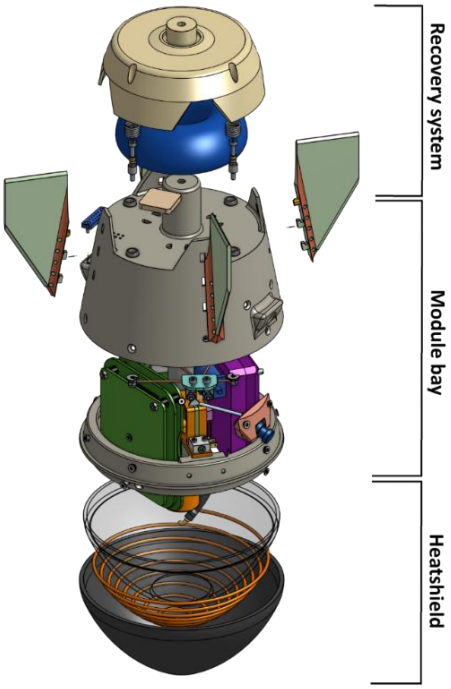

Fig. 12. Exploded view of the experimental module

The internal layout of FFU can be seen in Fig.13.

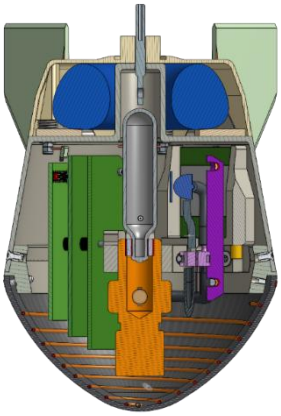

Fig. 13. Cross section of the experiment module

5.1 Recovery system

The parachute system (Fig. 14) is spring-loaded by four separate springs and held in place by a nylon line. A resistance wire is wound around the nylon and, once the deployment conditions are met, an electric current heats the wire and melts the nylon, releasing the upper cover. This cover is then ejected by the springs and functions as a pilot chute, pulling out the main parachute.

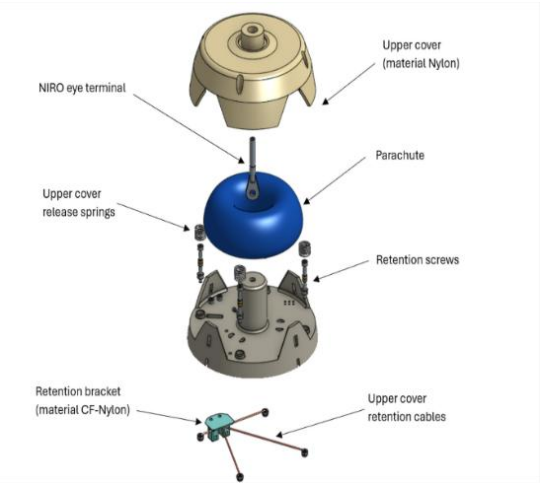

Fig. 14. Exploded view of the recovery system

Inside the cover are the release wire holders, which secure the wires used to trigger the mechanism. The cover release system is based on a nylon retention line: one end of the line is fixed with a restraint ball, while the other is attached to a tensioning pin that keeps the line under load (see Fig. 15). When commanded, the resistor wire cuts the nylon line, allowing the springs to push the cover away. at supersonic speeds (Mach 2–3).

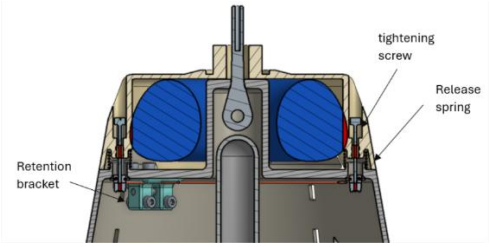

Fig. 15. Upper cover retention system

The parachute itself is packed in a C-shape configuration and connected to the FFU body with three 1 m long Dynema shock cords. Its suspension lines are temporarily secured by thread, which increases resistance during deployment, slows down canopy inflation, and reduces loads on the structure.

During release, the upper section of the parachute is connected to the cover with four Kevlar lines. As the cover is pulled away, these lines extract the main parachute. To ensure controlled inflation, a reefing ring is used to slow canopy opening and limit initial loads.

5.2 Module bay

The module bay is an integrated assembly that combines structural, electrical, and helium subsystems, each contributing to the overall performance of the FFU. It provides structural support, houses key electronics, and incorporates the helium cooling system used in the hybrid heatshield.

The main structural cover includes openings for the RMU connector and the onboard camera. It also provides holders for PCBs and a LoRa communication system. The cover is connected to the heatshield through the main support ring, which also secures the regulator holder and supports the three PCBs. This ring forms the primary interface between the heatshield and the module bay.

Entire structural assembly of FFU is depicted in Fig. 16.

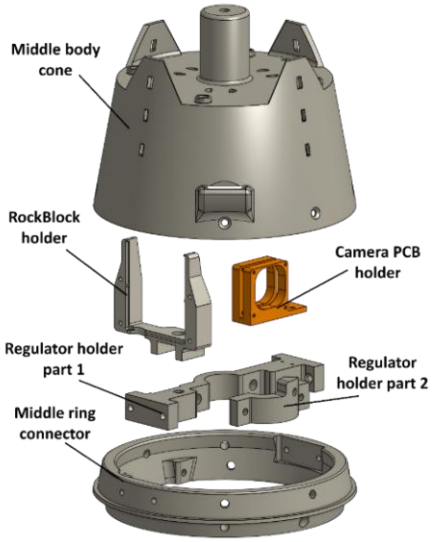

Fig. 16. Structural parts of module bay

For aerodynamic stability, four stabilization fins are mounted symmetrically around the capsule. The fins have a hexagonal shape with a 70° angle and a thickness of 3 mm, offering a balance between structural strength and aerodynamic efficiency.

Their surface area is maximized to shift the center of pressure (COP) upward relative to the center of gravity (COG), even at the expense of slightly higher drag. The fins are made of FR-4 glass fiber material, providing both strength and serving as supports for communication antennas (shown in Fig. 17). They are attached using hooks and glued from both sides for extra stiffness.

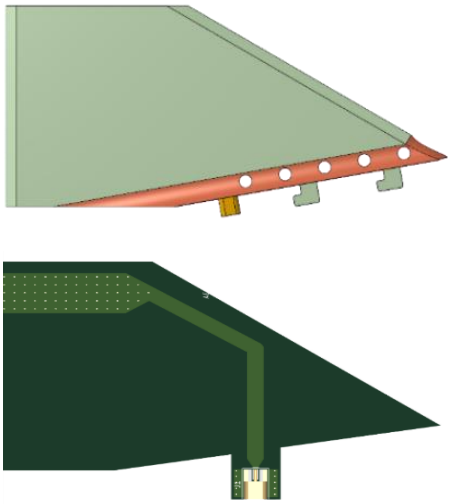

Fig. 17. Stabilisation fin design

The electrical system is mounted on the main structural cover. It includes three PCBs secured to the regulator holder, the onboard camera, communication modules, and power supply. Two 18650 Li-ion batteries are protected under a custom battery cover. A buzzer ON/OFF switch is integrated, allowing manual shutdown of the passive buzzer after capsule recovery. Additionally, a LoRa communication PCB developed by Team ShareON is placed inside the parachute compartment, just below the parachute, to provide recovery communication. The electrical components of the experiment are shown in Fig. 18.

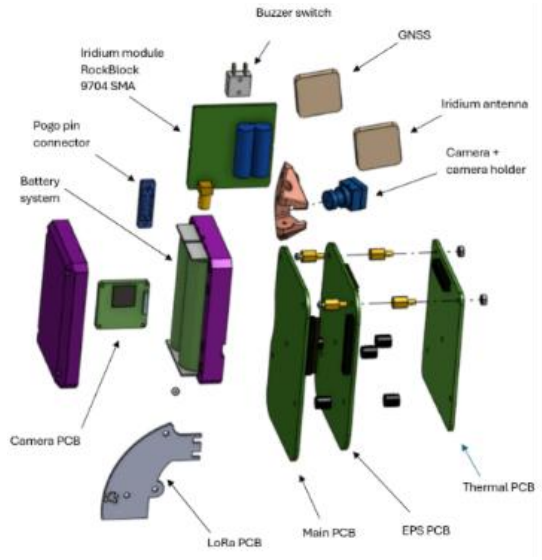

Fig. 18. Electrical components of the module bay

At the center of the module bay lies the helium system (Fig. 19), consisting of a disposable helium tank connected to a regulator and distribution assembly. The regulator, fixed by clamps to the support ring, links to a solenoid valve and flow-through pressure sensors that control and measure helium flow. The gas is then directed into a spiral pipe embedded below the regulator, distributing coolant into the heatshield structure.

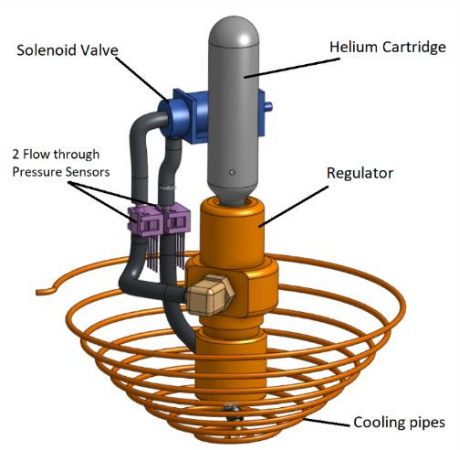

Fig. 19. Helium system components

A cone-shaped balance weight (Fig. 20) is mounted above the heatshield to shift the capsule's centre of gravity downward, improving aerodynamic stability. The weight is manufactured from a custom epoxy resin blended with tungsten powder in a 1:4 ratio, resulting in high density. This material composition ensures the required mass is concentrated in a compact geometry, optimizing capsule balance without excessive volume.

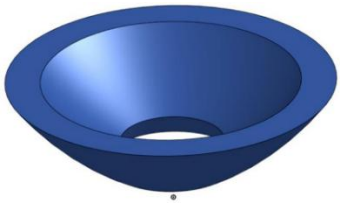

Fig. 20. Balance weight model

5.3 Heatshield

The heatshield is built from a carbon–epoxy composite (CEC) with an embedded cooling pipe system that allows helium to flow between its two layers. The helium exits through a short copper pipe protruding from the side of the heatshield.

The cooling pipes have an outer diameter of 2 mm and a wall thickness of 0.2 mm, made from standard C12200 copper tubing. Because of the small diameter and low elasticity, spring-back during shaping is minimal. To achieve precise geometry, the heatshield is manufactured using a combination of 3D-printed and machined aluminum molds: one for laminating the carbon composite and one for bending the piping

array. The layered design is shown in Fig.21.

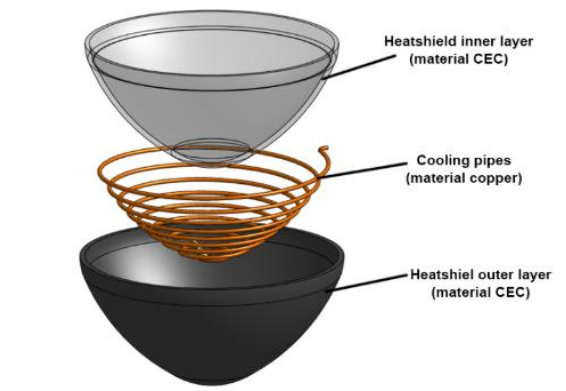

Fig. 21. Heatshield structure

Two versions of the heatshield material are used:

- **Carbon–Epoxy** (pre-flight mock-up): low-cost composite prepared in 3D-printed molds for mock-ups and pre-flight tests. Epoxy degrades above ~60–150 °C and does not ablate, so it is unsuitable for flight.
- **Carbon–Phenolic** (flight-ready): baseline flight material, resistant to high temperatures and capable of ablation. Requires autoclave curing at **130–180 °C** in aluminum molds.

For instrumentation, 37 PT100 sensors are laminated directly into the outer layer of the heatshield during production. These sensors are arranged in a 20 mm grid pattern to provide a detailed temperature map across the surface [5].

The hybrid heatshield makes use of two different protection methods:

- **Passive protection through the radiation of heat -** Based on the surface area of the heatshield and the emissivity of carbon fiber material the following radiative heat as a function of temperature is determined from Stefan-Boltzmann law. However, due to the minimal effect of radiative cooling, this effect is neglected.
- **Active protection through helium flow -** Helium is chosen as the cooling medium mainly for its use as pressurizing agent in propellant tanks. In a theoretical space mission, there is leftover helium inside empty fuel tanks that can be used to increase the effectiveness of re-entry systems. Moreover, helium has high thermal conductivity and thermal capacity and is non-reactive [6].

The exchange of heat is depicted in Fig. 37 in Appendix A.

6. Electronics

The electronics design of the HARTS experiment integrates all control, power, and measurement systems of the FFU and RMU. The FFU contains three PCBs: Core, Power and Thermal. An additional PCB is mounted on the RMU. Overview data flow diagram (Fig. 22) provides an overview of the interconnections between all included PCBs and the associated components connected to them.

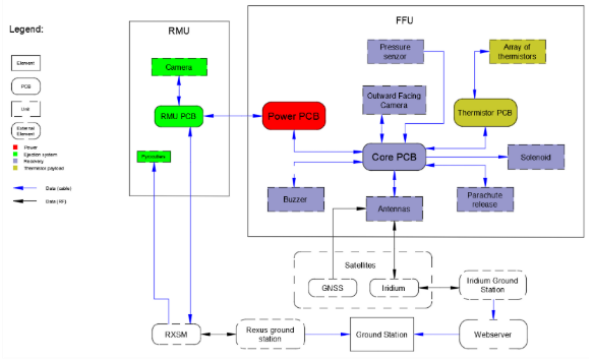

Fig. 22. Overview data flow diagram

All PCBs are designed from scratch by our electrical part of the team.

6.1 Core PCB

The Core PCB is responsible for the base functionality of the FFU including health monitoring, data-handling, timing, telemetry, telecommand, recovery and experiment interface. Its data flow diagram is shown in Fig. 23.

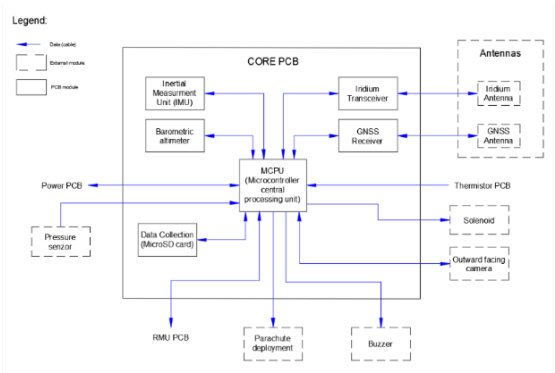

Fig. 23. Core PCB data flow diagram

6.2. Power PCB

Power PCB is responsible for handling the battery cells and providing all the different voltage levels. Its data flow diagram is shown in Fig.24.

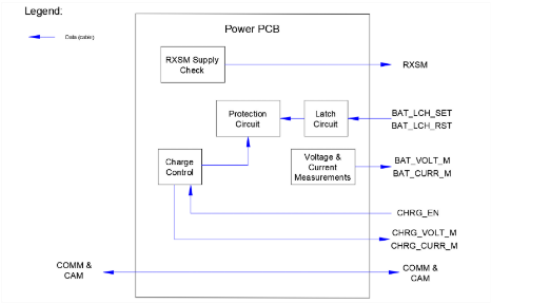

Fig. 24. Power PCB data flow diagram

The FFU is powered by two 3.6 V Li-ion cells in series. A protection circuit keeps the batteries within safe voltage limits, disconnecting them in case of over-voltage, deep discharge, or excess current. Charging is performed at 8.4 V / 670 mA (CV/CC mode). Battery health is monitored by voltage and current measurements to ensure sufficient charge for parachute deployment. A latch circuit maintains power even if the software crashes, with load connection controlled by set/reset signals.

6.3 RMU PCB

The RMU PCB serves as the interface between the RXSM and the FFU. It converts RS422 to RS485 communication and uses an optocoupler for galvanic isolation of the LO, SOE, and SODS signals, with SODS also triggering the camera. Its data flow diagram is shown in Fig.25.

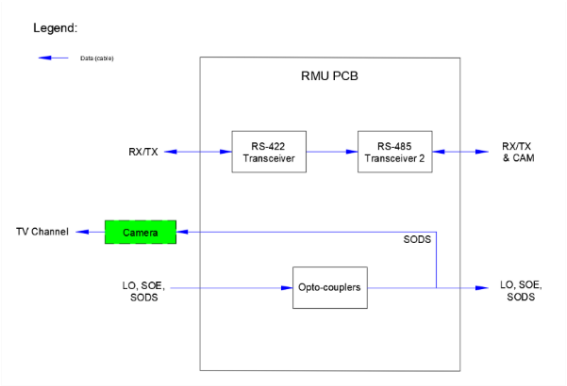

Fig. 25. RMU PCB data flow diagram

A RunCam Split 4 V2 camera is mounted on the RMU PCB to monitor ejection. It records 1080p/60 Hz video to a 128 GB SD card and can transmit live video via the REXUS TV channel (720×576). The camera powers on from an FFU signal and is kept active after ejection by a latching circuit.

6.4 Thermal PCB

The Thermal PCB processes data from 37 PT-100 sensors embedded in the heatshield, plus three inside the capsule, one on the batteries, and two for internal temperature monitoring. Sensor signals are routed through multiplexers, amplified, and then digitized before being sent to the STM32U575ZIT6 microcontroller on the Core PCB for processing [7]. Its data flow diagram is shown in Fig.26.

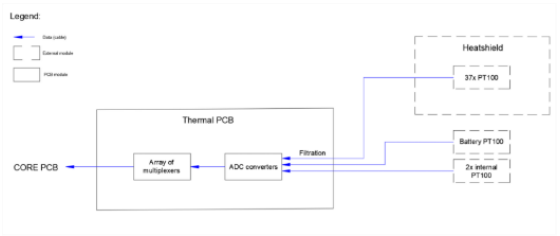

Fig. 26. Thermal PCB data flow diagram

7. Software

The experiment software manages all hardware components and subsystems throughout the mission lifecycle. Its tasks are divided into control, data acquisition, communication, and safety operations, ensuring reliable performance in every flight phase.

The communication system combines Iridium (1610–1626.5 MHz) and LoRa (868 MHz) modules.

- Iridium provides global coverage, transmitting minimal telemetry packets such as GNSS coordinates and health status.
- LoRa provides higher-rate local data transfer (10–20 kbit/s) to the ground station during descent. Antennas are integrated into PCB fins (21.6 cm monopoles), designed for aerodynamic protection and redundancy.

This dual-channel approach balances reliable long-range tracking with cost-effective, higher-resolution local telemetry.

The software runs under RTOS on the STM32U5 microcontroller. Tasks are prioritized, scheduled, and triggered by timers or interrupts.

- **Normal Mode** – Standard mission operation (waiting, launch, flight, landing).
- **Debug Mode** – Behaves as normal but enables console CLI and extended logging for ground testing.

Critical state flags (LO, SOE, SODS) control transitions between experiment phases. Flags are stored on the SD card for redundancy.

A Radio Silence Mode is used pre-launch, disabling

all communications and charging functions to comply with REXUS safety requirements. A custom switch reports Radio Silence status to the ground station.

7.1 Ground Station

The ground station software is the key element needed for interaction with the experiment. It displays received data transmitted by the FFU and enables competent experimenters to issue telecommands. It also obtains positional data of the FFU transmitted via the Iridium network and LoRa and takes care of saving all incoming data to a file.

The ground station interface is implemented as a web application [8]. The Graphical User Interface(GUI) can be seen in Fig 38 in Appendix A.

8. Simulations and testing

8.1 Trajectory predictions

The shape of the capsule is tested for its aerodynamic properties in all flight modes, including supersonic flight at atmosphere reentry, subsonic free fall and parachute landing. The basis of the atmospheric model was the change of coefficient of drag of the FFU capsule at different mach numbers. Fig.27 shows the resulting graph from CFD simulations in Fluent.

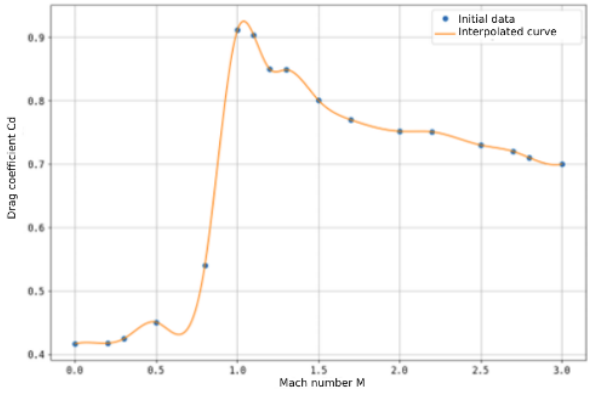

Fig. 27 Change of drag coefficient with mach number

A one–dimensional atmospheric re-entry simulation was developed using the 1976 U.S. Standard Atmosphere model in combination with the standard equations of motion. The trajectory of the Free-Falling Unit (FFU), assumed to have a mass of 3 kg, was computed for a ballistic descent initiated at an altitude of 85 km. The simulation includes both the free-fall dynamics and the deployment of the parachute recovery system. The resulting altitude–time profile is shown in Fig. 28.

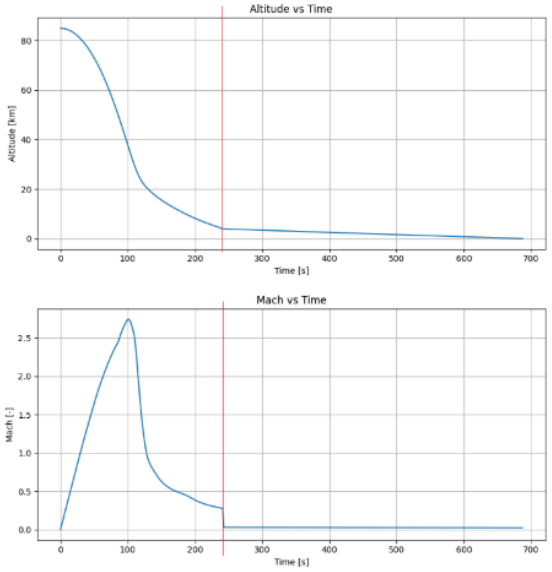

Fig. 28 FFU Predicted trajectory profile

8.2 Aerodynamic heating

Aerodynamic heating on the FFU surface is predicted using Eckert's reference enthalpy method for velocities up to Mach 3, where the heat flux at each surface station is calculated based on free-stream conditions, boundary layer properties, and local geometry. The FFU's outer contour is discretized into equally spaced points, and at each point the recovery temperature is determined, the Reynolds number is calculated using a modified form with local station length, and the Stanton number is obtained depending on whether the flow is laminar or turbulent. Flow regime is identified from the Reynolds number threshold, and compressibility corrections are applied.

The resulting approximate heat flux distribution along the surface is shown in Fig 29 and Fig 30.

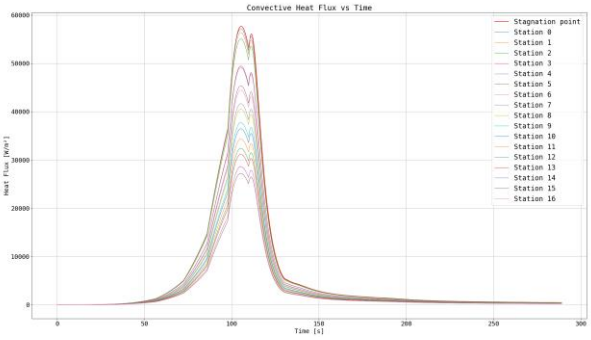

Fig. 29 Change of heatflux per station with time

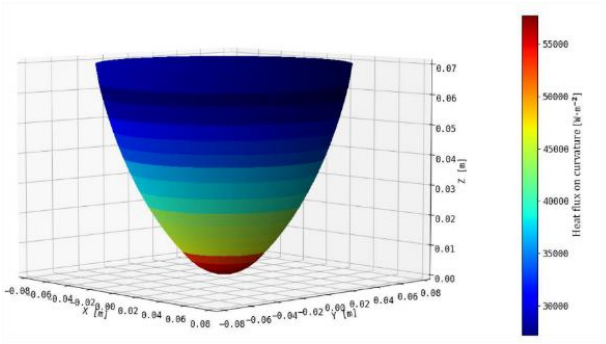

Fig. 30. Heat flux distribution along the FFU heatshield

8.3 Active cooling efficiency

The temperature difference between the active and passive heatshields can be clearly observed in the figures below. Time-dependent simulations of a free-fall trajectory from 85 km altitude, covering the interval from 85 s to 115 s after release, show that the introduction of helium cooling significantly reduces the thermal load. At the stagnation point, the inner wall temperature of the hybrid heatshield reached approximately 90 °C, compared to 126 °C for the purely passive design (See Fig.31) . This corresponds to a temperature reduction of 36 °C due to active cooling [10].

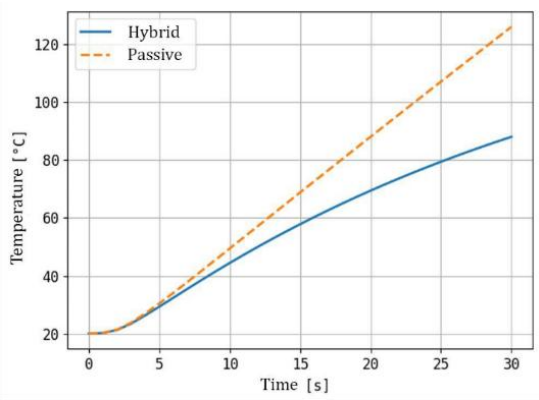

Fig. 31 Comparison of stagnation point temperature change with time for hybrid and passive heat shield

A heat map showing the distribution of temperatures at t=110s on the hybrid heatshield is shown in Fig. 32.

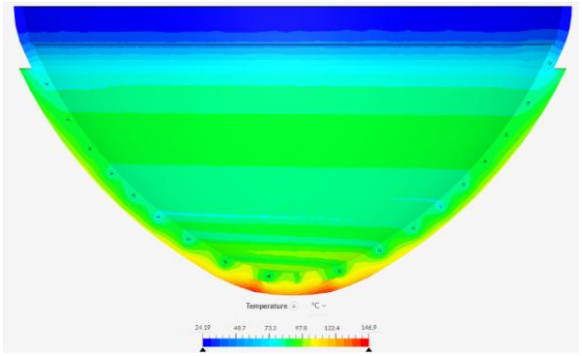

Fig. 32 Heat map of the hybrid heat shield in section

8.3 Descent thermal load

The CFD simulations of the FFU re-entry trajectory showed that the highest heat flux occurred at the stagnation point of the blunt capsule nose. At t = 115 s, the outer wall temperature reached a maximum of 162.4 °C (435.6 K), while the inner wall temperature peaked at 141.9 °C (415 K). Towards the capsule edges, heat flux decreased gradually.

At t = 202 s, shortly after parachute deployment, the minimum surface temperature of –3.6 °C (269.5 K) was recorded due to rapid cooling.

The internal components remained largely unaffected, as the dominant heat transfer occurred through the heatshield surface. Although the model did not include ambient air inside the capsule (limiting convection to the outer surface), conduction was found to be sufficient to distribute the absorbed heat.

Overall, the maximum temperatures remain well within the operational limits of the chosen heatshield material, confirming that passive thermal protection is sufficient for the mission and validating the thermal design under re-entry conditions [11].

The temperature at peak heat flux is shown in Fig. 33 and temperature before parachute deployment is shown in Fig. 34.

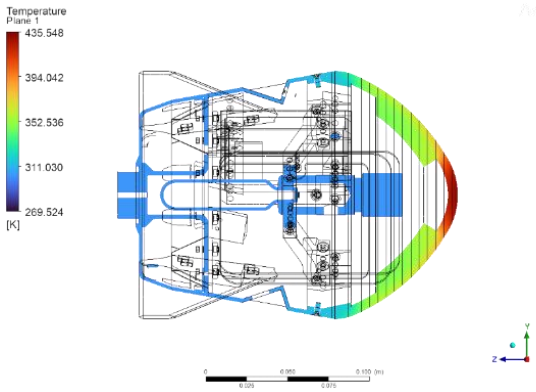

Fig. 33 Temperature distribution at t = 115 s

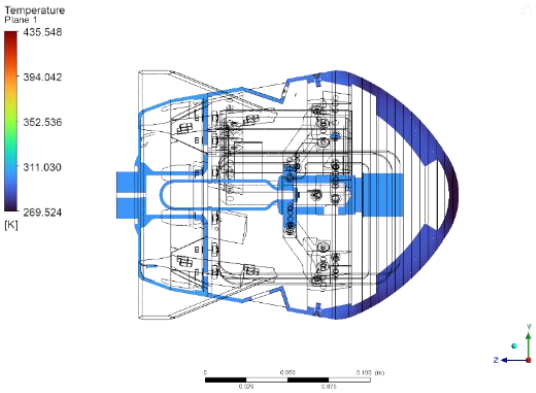

Fig. 34. Temperature distribution at t = 202 s

8.4 Parachute opening load

The parachute loading analysis determined a steady drag force of 2,420 N under terminal descent conditions, with a peak opening load of 3,630 N when accounting for the reefing factor. After applying a safety factor of 1.5, the resulting design load was set to 5,445 N.

For structural verification, simulations were performed in ANSYS Mechanical with a conservative applied force of 6 kN. The stress analysis focused on the weak points of the parachute baseplate, particularly the bridges between rope fastening holes.

The results (shown in Fig.35) indicate a maximum stress of 412.5 MPa, which remains below the yield strength of aluminium alloy 7075 (≈500 MPa). This confirms that the baseplate design can withstand parachute deployment loads with sufficient safety margin [12].

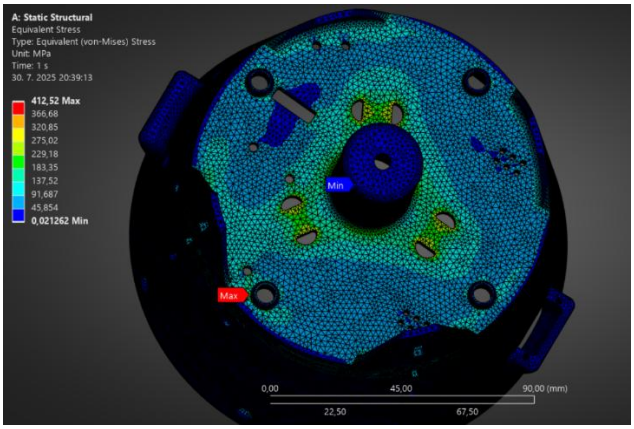

Fig. 35 Parachute Load Simulation Results

With the current parachute design and mass a terminal velocity at ground impact is expected to be ~ 9 m.s^{-1}.

In case of impact onto a hard surface a maximum stress of 262MPa has been calculated (Fig.36).

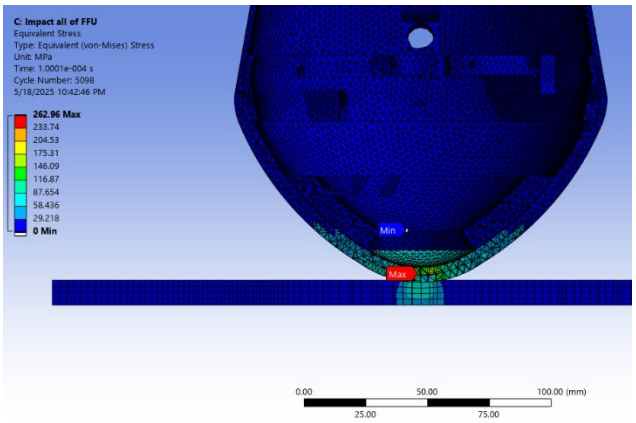

Fig. 36 Stress distribution at ground impact

With a tensile strength of ~45MPa, carbon phenolic is at a high risk of cracking in these locations in case of hard-surface landing due to the high stress experienced.

As such, further testing is needed with landing into both hard and soft surfaces to determine the FFU survivability, however, damage on impact would likely not cause damage to other structures [13].

9. Future and Beyond

In March 2026 we will conclude one and a half years of work. If the outcome is as expected and active cooling proves effective, we plan to continue our research. At present, doubts regarding helium cooling are present. Specifically, whether sufficient quantities can be stored in spacecraft tanks for descent cooling. While the thermal capacity of helium is superior to almost all other gases, its density is extremely low.

This results in low mass required but volumes exceeding the volume available inside the spacecraft. Other coolant gases have to be evaluated and simulated as a possible replacement for helium. This question will be addressed after our test, when the effectiveness of helium in the system can be verified.

One thing is certain. After completing this experiment, we will continue our research in this field with the goal of providing the industry with more reusable, cost-effective, and efficient thermal protection systems than those currently available on the market.

Conclusion

The HARTS experiment represents a novel step in the development of reusable thermal protection systems by integrating active helium cooling into a structural ablative heatshield. Designed, manufactured, and prepared by Slovak team HARTS within the REXUS/BEXUS programme, the project combines passive ablation with controlled coolant flow to address the limitations of current TPS technologies.

Through detailed design, subsystem integration, and numerical simulations, the feasibility of the hybrid concept has been demonstrated. The upcoming flight on REXUS 35 will provide the first real atmospheric re-entry data on the performance of helium-cooled carbon–phenolic composites, validating thermal, structural, and recovery subsystems in supersonic conditions.

Although challenges remain, such as verifying coolant performance and long-term material behaviour, the HARTS experiment is a decisive step toward demonstrating the viability of hybrid thermal protection. The upcoming flight will provide critical data on re-entry performance, offering a foundation on which more advanced concepts can be built. Beyond this milestone, our work is not finished, it is the starting point of a broader effort to push the boundaries of reusable spacecraft heatshield technology and open new pathways for safer and more sustainable access to space.

References

[1] Team HARTS, *RX3536_HARTS_SED_v3-0_5August2025*, Technical Document, Technical University of Košice, Aug. 2025, pp. 19–21.

[2] Team HARTS, *RX3536_HARTS_SED_v3-0_5August2025*, Technical Document, Technical University of Košice, Aug. 2025, pp. 21–66.

[3] Team HARTS, *RX3536_HARTS_SED_v3-0_5August2025*, Technical Document, Technical University of Košice, Aug. 2025, pp. 80–89.

[4] Team HARTS, *RX3536_HARTS_SED_v3-0_5August2025*, Technical Document, Technical University of Košice, Aug. 2025, pp. 71–73.

[5] Team HARTS, *RX3536_HARTS_SED_v3-0_5August2025*, Technical Document, Technical University of Košice, Aug. 2025, pp. 90–105.

[6] Team HARTS, *RX3536_HARTS_SED_v3-0_5August2025*, Technical Document, Technical University of Košice, Aug. 2025, p. 112.

[7] Team HARTS, *RX3536_HARTS_SED_v3-0_5August2025*, Technical Document, Technical University of Košice, Aug. 2025, pp. 106–110.

[8] Team HARTS, *RX3536_HARTS_SED_v3-0_5August2025*, Technical Document, Technical University of Košice, Aug. 2025, pp. 120–129.

[9] Team HARTS, *RX3536_HARTS_SED_v3-0_5August2025*, Technical Document, Technical University of Košice, Aug. 2025, pp. 307–312.

[10] Team HARTS, *RX3536_HARTS_SED_v3-0_5August2025*, Technical Document, Technical University of Košice, Aug. 2025, pp. 315–319.

[11] Team HARTS, *RX3536_HARTS_SED_v3-0_5August2025*, Technical Document, Technical University of Košice, Aug. 2025, pp. 322–324.

[12] Team HARTS, *RX3536_HARTS_SED_v3-0_5August2025*, Technical Document, Technical University of Košice, Aug. 2025, pp. 328–331.

[13] Team HARTS, *RX3536_HARTS_SED_v3-0_5August2025*, Technical Document, Technical University of Košice, Aug. 2025, pp. 331–332.

Appendix A: Additional Figures

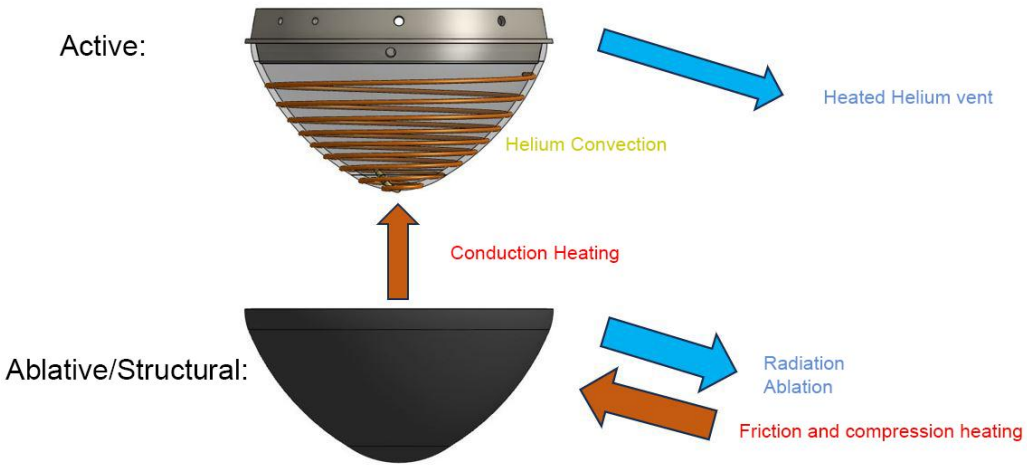

Fig. 37. Heatshield layers and heat flow indication

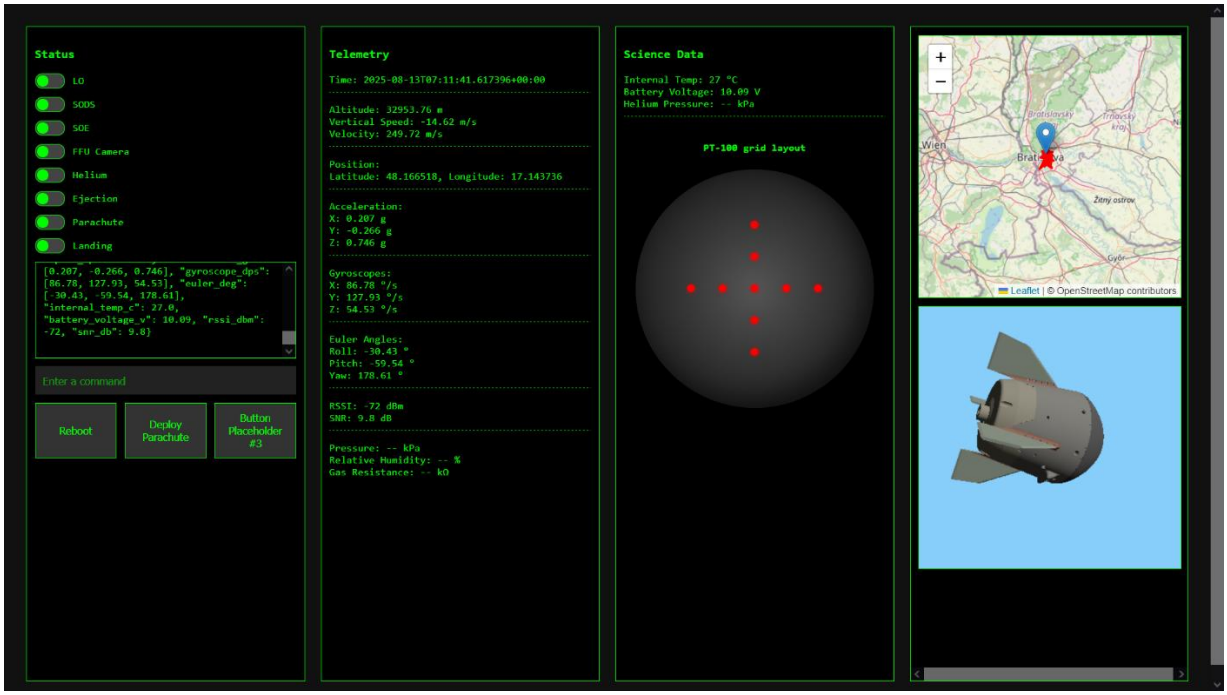

Fig. 38. Ground Station GUI Prototype